Available online at www.sciencedirect.com
SCIENCE DIRECT®
Journal of Solid State Chemistry 178 (2005) 2778–2790
JOURNAL OF SOLID STATE CHEMISTRY
www.elsevier.com/locate/jssc

Crystal structures, unusual magnetic properties and electronic band structures of $Cr_{5-x}Ti_xTe_8$

Zhong-Le Huang[a,*], Wolfgang Bensch[a], Diana Benea[b], Hubert Ebert[b]

[a]*Institute of Inorganic Chemistry, Christian-Albrechts-University Kiel, Olshausenstr. 40, D-24098 Kiel, Germany*
[b]*Department of Chemistry, LMU-Munich, Butenandstr. 5-13, D-81377 Munich, Germany*

Received 21 April 2005; received in revised form 25 May 2005; accepted 5 June 2005
Available online 21 July 2005

Abstract

The effect of substitution of the cation Cr by Ti in Cr_5Te_8 has been investigated with respect to its crystal structure, magnetic properties, and electronic structure. The compounds $Cr_{5-x}Ti_xTe_8$ ($x = 0$, 0.5, 1, 1.5, 1.85, 2, 3, 4, 5) were synthesized at elevated temperatures followed by slow cooling the samples to room temperature. The crystal structures have been refined with X-ray powder diffraction data with the Rietveld method. Three structural modifications are identified: monoclinic with space group $F2/m$ for $Cr_{5-x}Ti_xTe_8$ ($x = 0$, 0.5, 1, 1.5, 1.85), trigonal supercell with space group $P\text{-}3m1$ for $Cr_{5-x}Ti_xTe_8$ ($x = 2$, 3), and trigonal basic cell with space group $P\text{-}3m1$ for $Cr_{5-x}Ti_xTe_8$ ($x = 4$, 5). The structures of all these phases are related to the NiAs structure with full and deficient metal layers stacking alternatively along the c-axis.

The irreversibility in the field-cooled/zero-field-cooled magnetization with low field depends strongly on the Ti concentration x. Four types of magnetic states are distinguished: re-entrant ferromagnet for m-Cr_5Te_8, cluster-glass for m-$Cr_{4.5}Ti_{0.5}Te_8$ and m-Cr_4TiTe_8, antiferromagnetic for m-$Cr_{3.5}Ti_{1.5}Te_8$, and spin-glass for tr-$Cr_3Ti_2Te_8$, tr-$Cr_2Ti_3Te_8$, and $Cr_{0.25}TiTe_2$.

Accompanying spin polarized scalar-relativistic Korringa–Kohn–Rostoker band-structure calculations strongly support the observation that the crystallographic sites in the full metal layers are preferentially occupied and predict that Ti atoms have the preference to occupy the full metal layers. These compounds are predicted metallic. Results for the spin-resolved DOS and magnetic moments on each crystallographic sites are presented.

Keywords: Chromium chalcogenide; Cation substitution; Rietveld refinement; Low-field magnetization; Re-entrant spin-glass; Cluster-glass; Spin-glass; Relaxation; SP-SR KKR; Band-structure calculations

1. Introduction

The binary chromium chalcogenides and their pseudo-binary substitution derivatives have received much interest because of a rich variety of magnetic and transport property [1–12]. Some of them are predicted to be excellent candidates for half-metallic ferromagnets that are seen as a key ingredient in future high-performance spintronic devices [1]. Chemical substitution has significant influences on crystal structure, physical property, and electronic structure. By tuning chemical composition through chemical substitution, one can observe not only the transitions of crystal structures and physical properties between the boundary phases, but also one can expect unusual structural and physical property [2].

In binary chromium chalcogenides, tellurides ($Cr_{(1-x)}Te$, Cr_3Te_4, Cr_2Te_3 and dimorphic Cr_5Te_8) [3] are ferromagnetic (FM) with metallic conductivity; selenides ($Cr_{(1-x)}Se$, Cr_3Se_4, Cr_2Se_3, Cr_5Se_8) [4] and sulfides (CrS, Cr_5S_6, Cr_3S_4, Cr_2S_3, Cr_5S_8) [4b,5] are predominantly antiferromagnetic showing either metallic or semiconductor behavior. The existence of structural disorder and competing exchange interactions of opposite sign in these systems complex the elucidation of their magnetic behaviors. The lack of magnetic

*Corresponding author. Fax: +49 431 880 1520.
E-mail address: zlhuang@ac.uni-kiel.de (Z.-L. Huang).

0022-4596/$ - see front matter © 2005 Elsevier Inc. All rights reserved.
doi:10.1016/j.jssc.2005.06.004

investigation at low temperature and with low field leave the question of magnetic ground state in some of these systems to be addressed.

Among these compounds, we focused on the non-stoichiometric $Cr_{5\pm x}Q_8$ (Q = Te, Se, S) phases. After having studied the crystal structures of $Cr_{5\pm x}Te_8$ [6], $Cr_{5.095}Se_8$ [7], and $Cr_{5+y}S_8$ [8], we started to investigate their physical properties [9]. Furthermore, we are exploring the influence of anion- and cation-substitution in $Cr_{5\pm x}Te_8$ onto crystal structure and physical properties and electronic structure. Our preliminary study has shown that the substitution of one Te by one Se atom in $Cr_{5\pm x}Te_8$ induces the changes of the structures and magnetic properties [10].

We note that Ti_5Te_8 crystallizes in a trigonal system [11] and shows Pauli-paramagnetism like $TiTe_2$ [12] and Ti_3Te_4 [2e]. Hatakeyama et al. [13] reported recently the paramagnetic (PM) properties of $(Cr_{1-x}Ti_x)_5Te_8$ ($0 \leqslant x \leqslant 1$), where the samples were prepared by high-temperature solid-state reaction at 800 °C followed by quenching them in ice water. These compounds crystallize in trigonal basic cells.

In the pseudo-NiAs type structure of chromium chalcogenides, the arrangement of metal vacancies and the structural modification depends not only on the actual composition, but also on the heat treatment of sample preparation. Choosing different heat treatment mode of the sample preparation, one may obtain completely different results concerning the structure and physical properties. In this communication, we report on the effects of the cation substitution of Cr by Ti in Cr_5Te_8 phase onto the crystal structure and magnetic properties. The samples $Cr_{5-x}Ti_xTe_8$ ($x = 0$, 0.5, 1, 1.5, 1.85, 2, 3, 4, 5) were prepared by high-temperature solid-state reaction at 1000 °C for 5*d*, followed by cooling them with a rate of 100 °C/h to room temperature. After a discussion of the different structural modifications: monoclinic, trigonal supercell, and trigonal basic cell; we present the results of the magnetic measurements, especially the low-field magnetization; and discuss various behaviors like re-entrant FM, cluster-glass (CG), antiferromagnetic, spin-glass found in these materials. In the last section, the results of the SP-SR KKR band-structure calculations like preferential site occupation and density of states will be described. One of the most interesting aspects of this work is that the content of Ti in $Cr_{5-x}Ti_xTe_8$ as well as the heat treatment mode of the sample preparation have significant effects on the crystal structure and magnetic properties.

2. Experimental section

2.1. Synthesis

$Cr_{5-x}Ti_xTe_8$ ($x = 0$, 0.5, 1.0, 1.5, 1.85, 2.0, 3.0, 4.0, 5.0) phases were prepared by reaction of Cr (99.99%, Heraeus), Ti (99.5%, Chempur), and Te (99.999%, Retorte) powders in evacuated silica tubes ($\sim 10^{-5}$ mbar) according to the stoichiometric proportions. The starting mixtures were heated up to 420 °C at a rate of 100 °C/h and held at this temperature for 2 days. The temperature was then raised to 1000 °C with a rate of 100 °C/h and kept at this temperature for 5 days. Finally the temperature was lowered to room temperature at a maximum rate of 100 °C/h.

2.2. Composition analysis

The Cr, Ti, Te contents of the samples were determined by the Inductively Coupled Plasma (ICP) technique. The compositions of these samples are: Cr_5Te_8: $Cr_{5.02(2)}Te_8$; $Cr_{4.5}Ti_{0.5}Te_8$: $Cr_{4.527(1)}Ti_{0.464(3)}Te_8$; $Cr_4Ti_1Te_8$: $Cr_{3.946(3)}Ti_{1.100(3)}Te_8$; $Cr_{3.5}Ti_{1.5}Te_8$: $Cr_{3.54(4)}Ti_{1.43(1)}Te_8$; $Cr_{3.15}Ti_{1.85}Te_8$: $Cr_{3.16(1)}Ti_{1.846(5)}Te_8$; $Cr_3Ti_2Te_8$: $Cr_{3.03(6)}Ti_{1.99(4)}Te_8$; $Cr_2Ti_3Te_8$: $Cr_{2.028(1)}Ti_{2.982(1)}Te_8$; $Cr_1Ti_4Te_8$: $Cr_{1.022(2)}Ti_{3.970(7)}Te_8$; Ti_5Te_8: $Ti_{5.03(6)}Te_8$. The standard deviations are calculated on the basis of the numbers of analyses.

2.3. Powder X-ray diffraction and Rietveld refinement

X-ray powder patterns for the Rietveld refinements were collected on a STOE STADI P in transmission geometry using Cu-$K\alpha$ radiation ($\lambda = 1.54056$ Å) in the 2θ range of 10–100° with a position sensitive detector. The Rietveld refinements were done with the program package FULLPROF [14]. The background was interpolated linearly between the selected points. The profile of the reflections was modeled with a pseudo-Voigt function (3 parameters). Preferred orientation was treated using March's function. The atomic coordinates were refined and the values for B_{iso} with a common variable for all metal and all Te atoms. Based on the results of composition analysis, the ratio of (Cr + Ti):Te was fixed at 5:8. In addition, site occupation factors of partially occupied metal atom positions were refined with the constraint that the sum of metal atoms does not exceed 5 in the chemical formula. To get a better estimate of the accuracy of structural parameters the estimated standard deviations were multiplied by the serial correlation parameter after Berar's formula.

Because the X-ray diffraction cannot distinguish between Cr and Ti unambiguously, they are considered to be distributed over the possible crystallographic sites and the atomic form factor of Cr for Cr-rich phases with $x = 0.5$, 1.0, 1.5, 1.85, 2.0 or Ti for Ti-rich phase with $x = 3.0$ is chosen to represent both Cr and Ti in the refinements. For $x = 4.0$ phase, Ti atoms are in the full metal layers and Cr atoms in the metal deficient layers. The monoclinic structure was refined in space group $F2/m$ that is a non-conventional setting of $C2/m$. This setting is chosen for an easier visual comparison with

Table 1
Crystal data and structure refinement parameters of $Cr_{5-x}Ti_xTe_8$

Formula	$Cr_{5-x}Ti_xTe_8$				
x	0	0.5	1	1.5	1.85
Crystal system	Monoclinic				
Space group	$F\,2/m$				
a (Å)	13.5361(4)	13.4610(6)	13.4224(5)	13.4040(7)	13.3871(6)
b (Å)	7.8415(2)	7.8036(3)	7.7915(3)	7.7683(4)	7.7611(3)
c (Å)	12.0032(5)	12.1821(7)	12.3490(7)	12.4440(9)	12.4756(8)
ß (°)	90.473(2)	90.486(3)	90.612(2)	90.379(4)	90.421(3)
V (Å^3)	1274.02(8)	1279.60(11)	1291.39(10)	1295.72(14)	1296.15(12)
Z	4				
2θ (°)	10–100				
N_{obs}	285	280	293	282	262
N_{ref}	24	24	24	24	24
R_{wp}	5.54	7.72	5.31	8.48	5.32
R_e	4.43	6.51	3.85	6.78	3.54
GOF/χ^2	1.57	1.41	1.90	1.56	2.22
DW	1.1008	1.0802	0.7919	0.9874	0.7019
R_{Bragg}	5.55	6.18	4.22	6.18	4.44
R_F	10.1	9.33	7.26	7.23	8.55
Cr1–Cr3/Å	3.076(2)	3.112(1)	3.181(2)	3.166(2)	3.169(2)
Cr2–Cr4/Å	3.005(1)	3.049(1)	3.091(2)	3.115(1)	3.122(1)

Formula	$Cr_{5-x}Ti_xTe_8$		$Cr_{0.25}TiTe_2$	$Ti_{1.25}Te_2$
x	2	3	4	5
Crystal system	Trigonal supercell		Trigonal basic cell	
Space group	P-3m1		P-3m1	
a (Å)	7.7216(2)	7.7016(2)	3.8434(1)	3.8309(2)
b (Å)				
c (Å)	12.5192(6)	12.6372(5)	6.3703(3)	6.4076(4)
ß (°)				
V (Å^3)	646.43(4)	649.14(4)	81.493(1)	81.44(1)
Z	2		1	
2θ (°)	10–100	10–100		
N_{obs}	184	181	48	46
N_{ref}	22	22	12	12
R_{wp}	6.23	6.81	6.74	9.40
R_e	4.98	6.13	4.75	5.94
GOF/χ^2	1.56	1.23	2.01	2.50
DW	1.0054	1.1622	0.7499	0.5887
R_{Bragg}	4.44	3.90	3.87	6.81
R_F	11.4	9.44	3.92	5.57
M1–M3/Å	Cr1–Cr3	Ti1–Ti3	Ti1–Cr1	Ti1–Ti2
	3.152(2)	3.164(3)	3.185	3.204
M2–M4/Å	Cr2–Cr4	Ti2–Ti4		
	3.079(1)	3.154(2)		

Notes: The reliability factors have the standard definitions. DW is the Durbin–Watson statistics.

trigonal modifications with pseudo-NiAs type structure. The total refined parameters were 24, 22, and 12 for the monoclinic, the trigonal supercell, and the trigonal basic cell, respectively. The refinement results are listed in Table 1. Fig. 1 shows an example of the final Rietveld refinement plot for $Cr_{3.15}Ti_{1.85}Te_8$ with peak markers and difference plot at the bottom. Fig. 2 shows the minute differences of XRD patterns for monoclinic, trigonal supercell, and trigonal basic cell. Table 2 lists the atomic coordinates for representative $Cr_{5-x}Ti_xTe_8$ ($x = 1.85$, 2, 4).

2.4. Magnetic measurements

Magnetic measurements were conducted with a Quantum Design MPMS-7 device. The dc susceptibilities were measured in the temperature range of $4\,K \leqslant T \leqslant 300\,K$ with a field of 1 T for m-$Cr_{5-x}Ti_xTe_8$ ($x = 0$, 0.5, 1.0, 1.5) and 0.1 T for tr-$Cr_3Ti_2Te_8$, tr-$Cr_2Ti_3Te_8$, and tr-$Cr_{0.25}TiTe_2$. The susceptibility of the samples was also measured from 300 to 600 K on a Faraday balance with an external field of 1.5 T. The zero-field-cooled (ZFC) and field-cooled (FC)

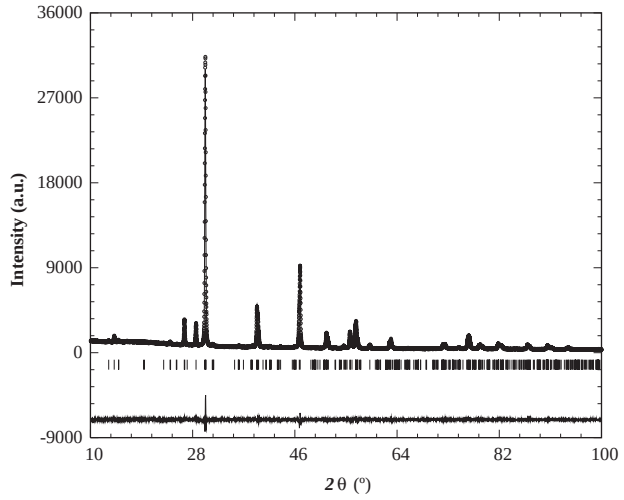

Fig. 1. Rietveld refinement plot for $Cr_{3.15}Ti_{1.85}Te_8$ with peak markers and difference plot at the bottom.

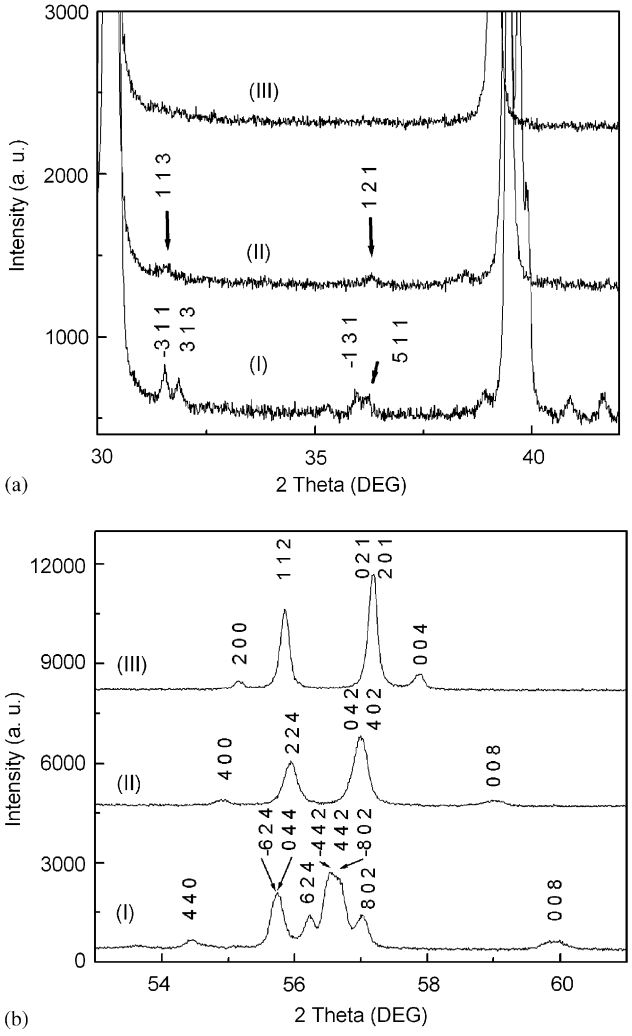

Fig. 2. (a, b) Local XRD patterns for monoclinic (I), trigonal supercell (II), and trigonal basic cell (III).

Table 2
Atomic coordinates for representative $Cr_{5-x}Ti_xTe_8$ ($x = 1.85$, 2, 4)

Atom	Site	x	y	z	B_{iso} (Å^2)	sof
m-$Cr_{3.15}Ti_{1.85}Te_8$						
Cr1	4*a*	0.0	0	0.0	5.1(2)	0.79(4)
Cr2	8*h*	0.25	0.269(3)	0.25	5.1(2)	1
Cr3	8*i*	−0.008(2)	0	0.254(2)	5.1(2)	1
Cr4	8*e*	0.25	0.25	0	5.1(2)	0.11(2)
Te1	8*i*	0.166(1)	0	0.132(1)	3.66(5)	1
Te2	8*i*	0.1659(9)	0.5	0.113(1)	3.66(5)	1
Te3	16*j*	0.4158(6)	0.249(1)	0.122(1)	3.66(5)	1
tr-$Cr_3Ti_2Te_8$						
Cr1	1*b*	0	0	0.5	5.7(2)	0.095(7)
Cr2	6*i*	0.494(2)	0.506(2)	0.246(2)	5.7(2)	1
Cr3	2*c*	0	0	0.248(4)	5.7(2)	1
Cr4	3*e*	0	0.5	0	5.7(2)	0.64(2)
Te1	2*d*	1/3	2/3	0.388(2)	4.03(4)	1
Te2	2*d*	2/3	1/3	0.131(3)	4.03(4)	1
Te3	6*i*	0.167(1)	0.833(1)	0.120(1)	4.03(4)	1
Te4	6*i*	0.835(1)	0.165(1)	0.375(1)	4.03(4)	1
tr-$Cr_{0.25}TiTe_2$						
Ti1	1*a*	0	0	0	5.1(2)	1
Cr1	1*b*	0	0	0.5	5.1(2)	0.25
Te1	2*d*	1/3	2/3	0.2606(7)	4.00(6)	1

magnetizations M_{ZFC} and M_{FC} were taken as follows. The system was cooled in zero field to 4.0 K, a field of 100 or 20 Oe was set immediately after $T = 4.0$ K was reached, and M_{ZFC} data taken on warming from 4.0 to 300.0 K; finally M_{FC} data recorded on cooling from 300.0 to 4.0 K with a field of 100 or 20 Oe.

2.5. Band-structure calculations

The electronic structure of the trigonal $Cr_{5-x}Ti_xTe_8$ systems was calculated self-consistently by means of the spin polarized scalar-relativistic Korringa–Kohn–Rostocker method in the atomic sphere approximation (ASA) mode [15–17]. The calculation method is based on the KKR–Green's function formalism that makes use of multiple scattering theory, as it has already been described in details elsewhere [18]. Exchange and correlation effects were treated within the framework of local density functional theory, using the parametrization of Vosko et al. [19]. The coherent potential approximation (CPA) is used to describe the random distribution of the Cr/Ti atoms and of the vacancies within the metal-layers [15,16,20,21].

3. Results and discussion

3.1. Crystal structure

The structures of $Cr_{5-x}Ti_xTe_8$ synthesized by slow cooling mode were refined from X-ray powder

diffraction with the Rietveld method. Three different structural modifications are distinguished (Table 1): monoclinic for $x = 0-1.85$; trigonal supercell for $x = 2-3$; and trigonal basic cell for $x = 4-5$. We note that samples prepared from the quenching mode crystallize only in trigonal basic cells [13]. In Fig. 2, the minute differences in the X-ray powder patterns are obvious. On the one hand, the differences are small, indicating the close relationship between these phases. On the other hand, the differences are obvious enough to be distinguished. Comparing the powder patterns of the trigonal basic cell with that of the trigonal supercell extra weak reflections (113) and (121) occur for the latter phase. Reducing the symmetry from the trigonal supercell to the monoclinic cell, the splitting of several reflections especially at high scattering angles are observed. For example, the reflections (042) and (402) in trigonal supercell are split into ($\bar{6}24$), (044), (624), ($\bar{4}42$), (442), ($\bar{8}02$), (802) in monoclinic symmetry.

The variations of lattice parameters (a, b, c, V for monoclinic; a, c, V for trigonal) with Ti content x in $Cr_{5-x}Ti_xTe_8$ phases are presented in Fig. 3. With increasing Ti concentration the monoclinic cell parameters (a and b) and the trigonal cell parameter a decrease monotonously; while the cell parameter c and volume V increase. Such trends imply the contraction of the ab plane and the elongation of the c-axis. The effect of the c-axis elongation is larger than the ab plane contraction, resulting in a net increase of unit cell volume with increasing Ti concentration. At the boundary of the monoclinic and the trigonal supercell, a discontinuity is found for both the cell volume V (Fig. 3b) and the ab plane cell parameters (b for monoclinic and a for trigonal supercell, Fig. 3a). The increase of V is due to the larger ionic or atomic radius of titanium Ti(III) or Ti(IV) than those of Cr [22]. The transition from monoclinic to trigonal supercell may be due to the increase of Ti concentration, and thus the induced increase of V. Such boundary may predict that when the temperature is raised for the monoclinic phase near the boundary, the monoclinic phase may transform into the trigonal supercell because of the temperature-induced volume enlargement.

For monoclinic Cr_5Te_8, four different crystallographic sites for metal atoms are found as during a single crystal study of monoclinic Cr_5Te_8 [6]: two within the fully occupied metal atom layers (Cr2 on 8h and Cr3 on 8i) and two in the partially populated metal layer (Cr1 on 4b and Cr4 on 8e), with a significant preference for site 4b. For monoclinic $Cr_{5-x}Ti_xTe_8$ ($x = 0.5$, 1.0, 1.5, 1.85), a slightly different picture was observed. Starting with Cr in 8h and 8i we found the highest residual electron densities in the positions 4a and 8e, whereas no significant electron densities could be observed on site 4b. Hence the Cr atoms occupy four different sites: two within the fully occupied metal

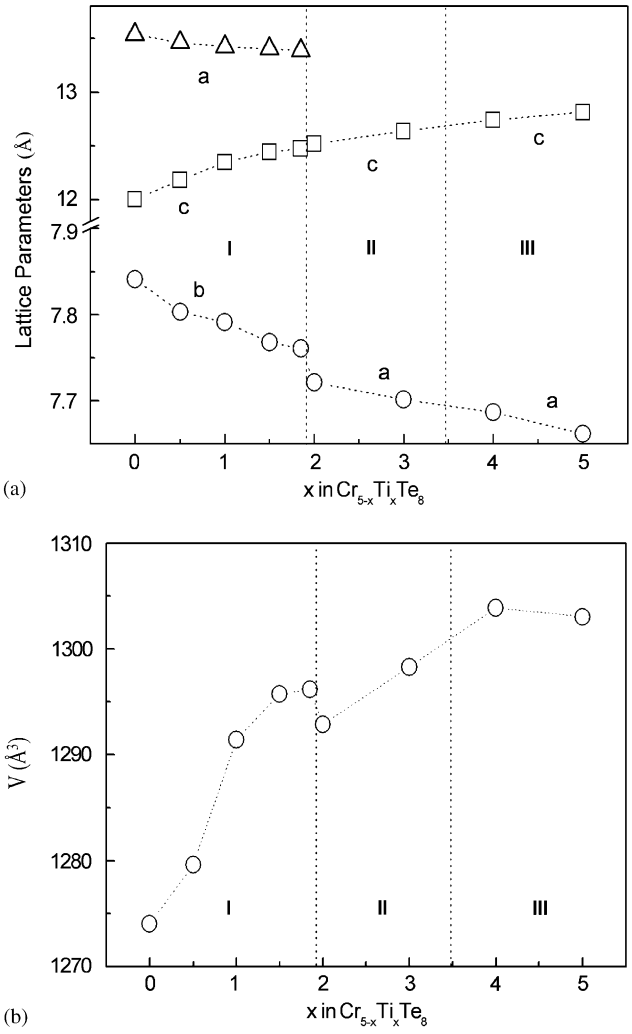

Fig. 3. (a, b) Variations of lattice parameters (a, b, c, V) on Ti concentration x in $Cr_{5-x}Ti_xTe_8$ phases. Region I is for monoclinic; region II for trigonal supercell; region III for trigonal basic cell. Those for trigonal basic cells are doubled for easy comparison. The dotted lines are used for eyes' guide.

atom layers (Cr2 on 8h and Cr3 on 8i) and two in the partially populated metal layer (Cr1 on 4a and Cr4 on 8e), with a significant preference for site 4a. This arrangement of the metal atoms within the unit cell is shown in Fig 4(a). The only difference between m-Cr_5Te_8 and m-$Cr_{5-x}Ti_xTe_8$ is that Cr1 occupies the 4b site for the former and 4a site for the latter. We note also that in the V_5X_8 structure type [23], the metal atoms within the partially occupied metal layers are exclusively located on site 4a. These examples present a rich diversity of the vacancy ordering in the M_5X_8 crystal structures.

For trigonal $Cr_{5-x}Ti_xTe_8$ ($x = 2$, 3) with the supercell, four different crystallographic sites are present as found during a single crystal study of trigonal Cr_5Te_8 [6]. Two of them, 6i site for Cr2 and 2c site for Cr3, constitute the fully occupied metal layers; the other two, 1b site for Cr1

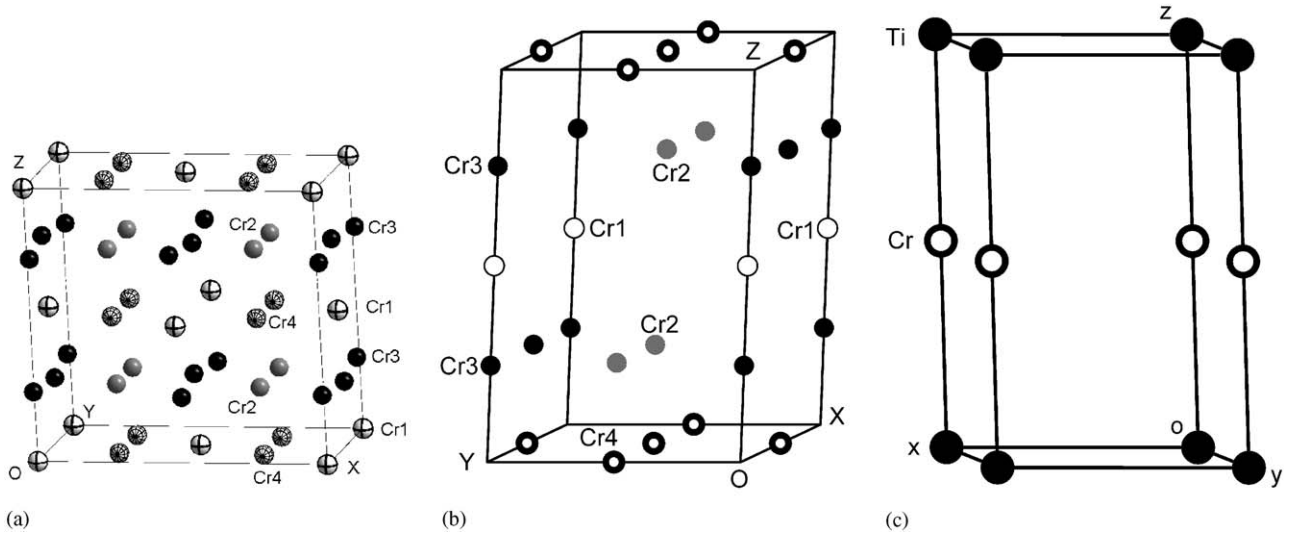

Fig. 4. Arrangements of the Cr atoms within the unit cells: (a) for m-$Cr_{5-x}Ti_xTe_8$ ($x = 0.5, 1.0, 1.5, 1.85$); (b) for tr-$Cr_{5-x}Ti_xTe_8$ ($x = 2.0, 3.0$) with supercell; and (c) for tr-$Cr_{0.25}TiTe_2$ with basic cell. The Te atoms are omitted for clarity. The sites Cr1 and Cr4 in m-$Cr_{5-x}Ti_xTe_8$ and tr-$Cr_{5-x}Ti_xTe_8$, and Cr in $Cr_{0.25}TiTe_2$ are only partially occupied.

and 3*e* site for Cr4 with a significant preference for site 3*e*, makes up the metal deficient layers.

For trigonal $Cr_{5-x}Ti_xTe_8$ ($x = 4, 5$) with the basic cell the structure can be compared to the CdI_2 structure and the formula is thus reduced to $Cr_{0.25}TiTe_2$ and $Ti_{1.25}Te_2$. Site 1*a* is fully occupied by Ti atoms and site 1*b* is partially occupied by the rest of Cr or Ti atoms; the anions are on site 2*d*. For $x = 4$, three models [(a) Cr and Ti atoms are statistically distributed on 1*a* and 1*b*; (b) Cr atoms represent both Cr and Ti and occupy 1*a* and 1*b*; (c) Ti atoms on 1*a* and Cr atoms on 1*b*] are chosen to refine the structure and model (c) yields the best results.

The crystal structures of $Cr_{5-x}Ti_xTe_8$ are shown in Fig. 4. All structures can be viewed as a derivative of the hexagonal NiAs-type structure with metal vacancies. The Te atoms are hexagonal close packed and the metal atoms occupy the octahedral interstices. Thus the full and deficient metal layers stack alternatively along the *c*-axis. Within the layers, the $CrTe_6$ octahedra share common edges, while $CrTe_6$ octahedra in neighbored layers have common faces and relatively short Cr–Cr separations along the crystallographic *c*-axis result. These short Cr–Cr interatomic distances are listed in Table 1, ranging from 3.00 to 3.20 Å. Such short Cr–Cr distances along the *c*-axis indicate weak bonding interactions between these metal centers. The partial occupancy character of metal atoms in the metal deficient layers implies that no infinite Cr–Cr atom chains are present. Another interesting feature of these structures is the differences of M–Te distances in the full metal layers and in the deficient metal layers. The M–Te distances for m-$Cr_{3.15}Ti_{1.85}Te_8$, tr-$Cr_3Ti_2Te_8$, and tr-$Cr_{0.25}TiTe_2$ are listed in Table 3. They can be classified into two groups. One is in the fully occupied metal layers; the other is in the metal deficient layers. Those in the full layers are obviously longer than those in the deficient layers. For example, the M–Te bonds in tr-$Cr_{0.25}TiTe_2$ are 2.7713 and 2.6925 Å in the full and deficient layers, respectively. In an ionic picture, the electronic situation requires the coexistence of M^{3+} and M^{4+} in M_5Te_8. The smaller M–Te distances imply smaller M^{n+} radius and may be considered as an indication for a higher oxidation state of M in the deficient layers. With increasing Ti content the cation substitution of Cr by Ti in Cr_5Te_8 has led to the

Table 3
Selected M–Te interatomic distances (Å) for m-$Cr_{3.15}Ti_{1.85}Te_8$, tr-$Cr_3Ti_2Te_8$, and tr-$Cr_{0.25}TiTe_2$

m-$Cr_{3.15}Ti_{1.85}Te_8$	Average	tr-$Cr_3Ti_2Te_8$	Average
Cr1–Te2 2*x* 2.757(5)		Cr1–Te4 6*x* 2.710(5)	2.710
Cr1–Te3 4*x* 2.720(5)	2.732		
		Cr2–Te1 1*x* 2.808(12)	
Cr2–Te1 2*x* 2.789(9)		Cr2–Te2 1*x* 2.717(12)	
Cr2–Te2 2*x* 2.713(8)		Cr2–Te3 2*x* 2.697(10)	
Cr2–Te3 2*x* 2.747(4)	2.750	Cr2–Te4 2*x* 2.797(10)	2.752
Cr3–Te1 1*x* 2.784(12)		Cr3–Te3 3*x* 2.748(7)	
Cr3–Te2 1*x* 2.700(12)		Cr3–Te4 3*x* 2.723(7)	2.736
Cr3–Te3 2*x* 2.739(9)			
Cr3–Te3 2*x* 2.763(9)	2.748	Cr4–Te2 2*x* 2.769(8)	
		Cr4–Te3 4*x* 2.688(8)	2.715
Cr4–Te1 2*x* 2.791(4)			
Cr4–Te2 2*x* 2.653(4)		tr-$Cr_{0.25}TiTe_2$	
Cr4–Te3 2*x* 2.683(4)	2.709	Ti1–Te1 6*x* 2.7713(9)	2.7713
		Cr1–Te1 6*x* 2.6925(9)	2.6925

Note: M–M distances are listed in Table 1. Estimated standard deviations are given in parentheses.

structural transition from monoclinic to trigonal supercell, and then to a trigonal basic cell. These results are completely different from those reported in Ref. [13] where the samples were prepared by the quenching mode and crystallize in trigonal basic cells. The differences of these structures are reflected by the different distribution patterns of the metal atoms in the metal deficient layers. The randomness of Cr and Ti distribution, the ratio of Cr/Ti concentrations, and the distribution patterns of magnetic ions will have great effects on the magnetic properties of these materials as discussed below.

3.2. Magnetic properties

The temperature dependence of the inverse susceptibilities for $Cr_{5-x}Ti_xTe_8$ ($x = 0$, 0.5, 1, 1.5, 2, 3, 4) materials are plotted in Fig. 5. In all cases, $\chi(T)$ obeys the Curie–Weiss law $\chi(T) = C/(T - \theta_P)$ in the high-temperature range. Note that the data are not corrected for the PM contribution of the conducting electrons. The fitting parameters, the effective magnetic moment μ_{eff} and the Weiss constants θ_P are listed in Table 4. The effective magnetic moments μ_{eff} are between 3.9 and 4.3 μ_B per Cr atom, slightly larger than the expected value 3.87 μ_B for spin-only Cr^{3+}. In the temperature region between 300 and 600 K the magnetic moments per Cr atom are still large and amount to about 4.20 μ_B for all compounds. This is quite unusual for Cr^{3+}, but was often observed for chromium chalcogenides [24]. It may be due to the electron transfer from Te to Cr through *d–p* hybridization [25]. As pointed out above, in an ionic picture the coexistence of Cr^{3+} (d^3) and Cr^{4+} (d^2) is required for Cr_5Te_8 and $Cr_{4.5}Ti_{0.5}Te_8$, and one would assume that the effective magnetic moment is slightly smaller than 3.87 μ_B. The Weiss constants are quite large and positive at the beginning of the series indicating strong FM exchange interactions. But θ_p decreases monotonously with increasing Ti content. The value for θ_p is only 4 K for $Cr_{0.25}TiTe_2$, implying very weak FM interactions.

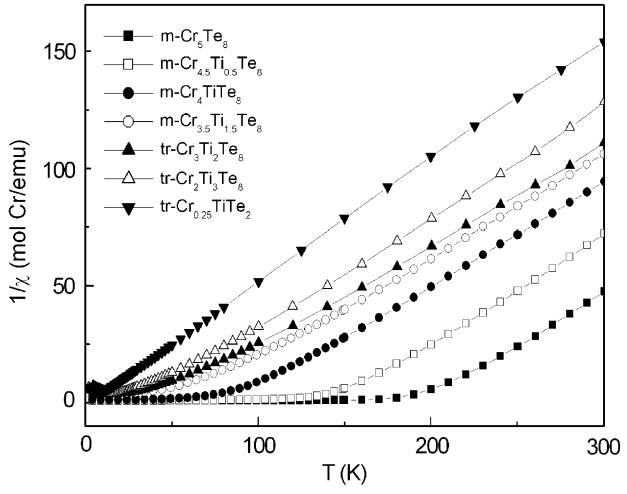

Fig. 5. Temperature dependencies of the inverse magnetic susceptibilities at a field of 1 T for m-Cr_5Te_8, m-$Cr_{4.5}Ti_{0.5}Te_8$, m-Cr_4TiTe_8, and m-$Cr_{3.5}Ti_{1.5}Te_8$ and 0.1 T for $Cr_3Ti_2Te_8$, $Cr_2Ti_3Te_8$, and $Cr_{0.25}TiTe_8$.

Table 4
Magnetic parameters for $Cr_{5-x}Ti_xTe_8$

x	μ_{eff}[a] (μ_B/Cr)	θ_p[a] (K)	H[a] (T)	T_{min}/T_{max}[a] (K)	T_c (K)	T_f (K)
0	4.2	196	1	230/300	160	9[b]
0.5	4.1	149	1	200/300	129	111
1	4.2	88	1	150/300	74	52
1.5	4.2	61	1	150/300	29[c]	—
2	4.3	45	0.1	120/300	—	23
3	4.1	37	0.1	140/300	—	16
4	3.9	4	0.1	50/200	—	9

[a] μ_{eff} and θ_p are the results of fits of Curie–Weiss law to the magnetic susceptibilities. H is the applied field. T_{min}/T_{max} indicate the range of the fit.
[b] T_R.
[c] T_N instead T_c.

In order to answer the question of magnetic ground states of these materials, the temperature dependence of ZFC and FC magnetizations with low fields were measured. Fig. 6 shows the magnetizations M_{ZFC} and M_{FC} for $Cr_{5-x}Ti_xTe_8$ ($x = 0$, 0.5, 1, 1.5, 2, 3, 4) materials, respectively. Here we define the quasi-critical temperature or Curie temperature T_c and the freezing temperature T_f as follows (Fig. 7, Table 4): T_c is the temperature where the minimum of the $d\chi_{(ZFC)}/dT$ vs. T curve occurs, while T_f is the temperature at which ($d\chi_{(ZFC)}/dT$) crosses the zero line. From Fig. 6, one can find four different types of M_{ZFC} and M_{FC} curves, representing four different types of magnetic interactions.

The M_{ZFC} and M_{FC} for m-Cr_5Te_8 are shown in Fig. 6(a). The values for T_c and the re-entrant temperature are 160 and 9 K, respectively (Table 4). From Fig. 6(a) one observes first a transition from the PM state to a long-range FM ordered state, which is signaled by a sharp increase of both the ZFC and FC magnetizations below T_c. This transition has been reported by our former study [9]. The interesting feature of the low-field magnetization is the magnetic irreversibility observed in the separation of the FC and ZFC curves below T_c. This irreversibility, the difference of $M_{FC}-M_{ZFC}$, starts to appear below 120 K and increases first slowly just below 120 K. Then it increases dramatically with decreasing temperature below 9 K (Fig. 6(a)). The irreversible effect of magnetization at the second step, i.e., below 9 K, clearly indicates the occurrence of spin-glass behavior. This is typical for a re-entrant spin-glass (RSG) that is defined by the appearance of a spin-glass state at a

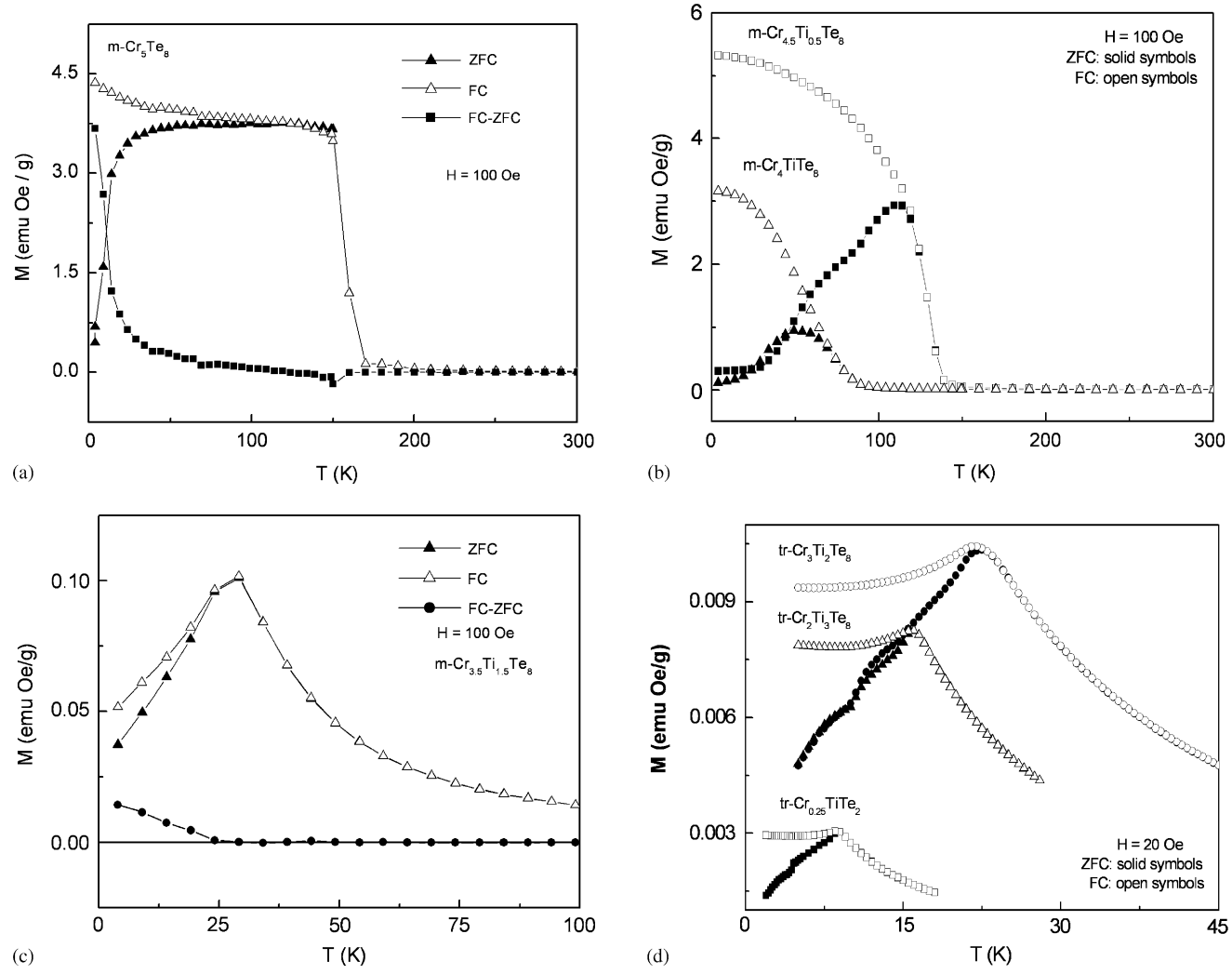

Fig. 6. Temperature-dependent M_{ZFC} and M_{FC} for m-Cr_5Te_8 (a), m-$Cr_{4.5}Ti_{0.5}Te_8$ and m-Cr_4TiTe_8 (b), m-$Cr_{3.5}Ti_{1.5}Te_8$ (c), and tr-$Cr_3Ti_2Te_8$, tr-$Cr_2Ti_3Te_8$, and tr-$Cr_{0.25}TiTe_2$ (d).

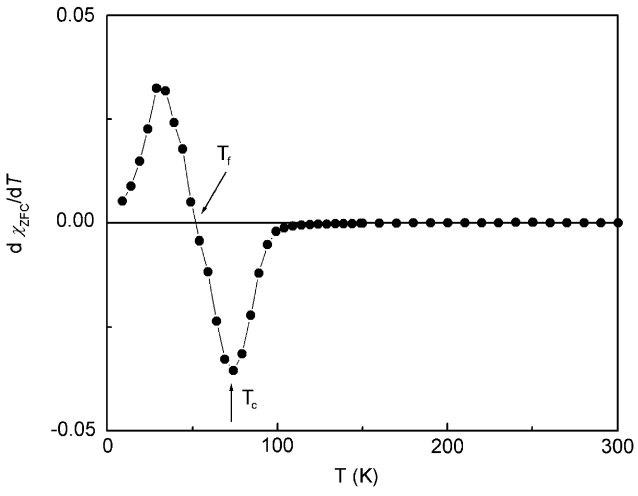

Fig. 7. [$d\chi_{(ZFC)}/dT$] as a function of temperature for m-Cr_4TiTe_8 with a field of 100 Oe.

temperature lower than that of the long-range-ordered state and experimentally characterized by a rapid drop of the low-field magnetization at T_R, below which an appreciable history- and time-dependent magnetization appear. Such behavior has been reported for systems like alloys Fe–Al, Au–Fe, Ni–Mn [26], oxides [27], and chalcogenides [28], which were interpreted and supported by the Gabay–Toulouse model [29]. In this model, it is predicted that in the RSG phase, FM long-range order is coexistent with spin-glass behavior [29].

The M_{ZFC} and M_{FC} for m-$Cr_{4.5}Ti_{0.5}Te_8$ and m-Cr_4TiTe_8 are shown in Fig. 6(b). The Curie temperature and the freezing temperature (T_c, T_f) are (129, 111) K and (74, 52) K for m-$Cr_{4.5}Ti_{0.5}Te_8$ and m-Cr_4TiTe_8, respectively (Table 4). The M_{ZFC} curve shows a broad maximum at T_f, and the M_{FC} curve is nearly flat above T_c and increases drastically with decreasing the temperature below T_c. Finally; the magnetization tends to

level off at lower temperature. Such a behavior is different from that for a canonical spin-glass. For spin-glasses, the FC curve is almost flat below the freezing temperature [30], but in our case it continues to rise. It is also different from the case observed for m-Cr_5Te_8 (see above), in which the irreversibility occurs at temperatures far below T_c. For m-$Cr_{4.5}Ti_{0.5}Te_8$ and m-Cr_4TiTe_8, the irreversibility occurs just below T_c. In our former study we reported the effect of the anion substitution of Cr_5Te_8 [10], which has led to the formation of $Cr_{(1+x)}Q_2$ (Q = Te, Se; Te:Se = 7:1) phases crystallizing in trigonal basic cells and showing the same irreversibility as described above. Similar behavior has been reported and interpreted as CG properties in the following materials: $La_{0.7}Sr_{0.3}Mn_{0.7}Co_{0.3}O_3$ [31(a)], $La_{0.5}Sr_{0.5}CoO_3$ [31(b), (c)], $Fe_{1/3}TiS_2$ [31(d)], $Ca_{0.9}Sm_{0.1}MnO_3$ [31(e)], and the molecule-based magnet $K_{1-2x}Co_{1+x}[Fe(CN)_6]\cdot yH_2O$ [31(f), (g)]. The rapid rise in magnetization around T_c may be associated with the occurrence of finite range FM ordering, forming spin clusters near the quasi-critical temperature, the clusters are randomly frozen as T is further decreased.

Fig. 6(c) shows the temperature dependence of M_{ZFC} and M_{FC} for m-$Cr_{3.5}Ti_{1.5}Te_8$. Both curves have a broad maximum around T_N (= 29 K), which may suggest the set-in of short-range antiferromagnetic interactions. The irreversibility appears just below T_N. The difference of $M_{FC}-M_{ZFC}$ increases slowly with decreasing temperature. No abrupt increase in $M_{FC}-M_{ZFC}$ is observed at lower temperature, suggesting the absence of spin-glass behavior.

In Fig. 6(d) the temperature dependence of M_{ZFC} and M_{FC} for tr-$Cr_3Ti_2Te_8$, tr-$Cr_2Ti_3Te_8$, and tr-$Cr_{0.25}TiTe_2$ are displayed. The curves are characteristic for a canonical spin-glass in which the FC curve is almost flat below the freezing temperature [30]. The freezing temperatures for tr-$Cr_3Ti_2Te_8$, tr-$Cr_2Ti_3Te_8$, and tr-$Cr_{0.25}TiTe_2$ are 23, 16, and 9 K, respectively.

Using the Curie temperature T_c, the re-entrant temperature T_R and the freezing temperature T_f, the magnetic phase diagram for $Cr_{5-x}Ti_xTe_8$ is constructed and is presented in Fig. 8. From this figure four types of magnetic states at low temperature can be distinguished. With increasing Ti content first the re-entrant FM behavior of m-Cr_5Te_8 is observed; then CGs are found for m-$Cr_{4.5}Ti_{0.5}Te_8$ and m-Cr_4TiTe_8; followed by the antiferromagnetic property of m-$Cr_{3.5}Ti_{1.5}Te_8$; and finally spin-glass behavior for tr-$Cr_3Ti_2Te_8$, tr-$Cr_2Ti_3Te_8$, and tr-$Cr_{0.25}TiTe_2$.

In order to explain the observed magnetic properties, the following chemical, structural, and magnetic exchange mechanisms must be considered. In addition one should keep in mind that the magnetic properties of Ti tellurides are dominated by a temperature independent Pauli paramagnetism suggesting that the Ti atoms are magnetically silent in the title compounds: (i) the

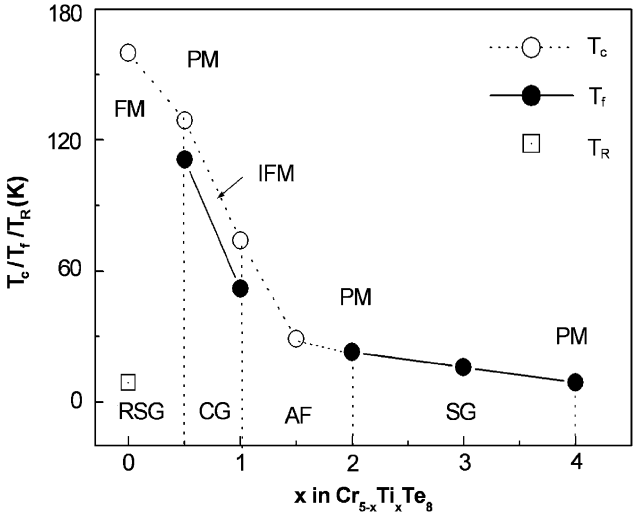

Fig. 8. Magnetic phase diagram. Dotted and solid lines are used as guides for the eyes. PM: paramagnetism; FM: ferromagnetism; RSG: re-entrant spin-glass; IFM: intra-cluster FM; CG: cluster-glass; AF: antiferromagnetism; SG: spin-glass.

concentration of Ti: it directly influences the concentration of magnetic moments in the relevant compound. The Curie temperature thus decreases with the increase of Ti content (Fig. 8); (ii) intra-layer Cr–Te–Cr FM superexchange: within the *ab* plane, the Cr–Cr distances are larger than 3.75 Å and thus there is no direct exchange interaction within the layers. According to Kanamori and Goodenough [32] the intra-layer FM superexchange occurs on the Cr sublattice via 90° Cr–Te–Cr σ/π bonding which links a half-filled t_{2g} (π) on one Cr with an empty e_g (σ) level on the other. Large deviations from 90° angle weaken the FM exchange; (iii) inter-layer direct Cr–Cr exchange: the short Cr–Cr distances (3.00–3.20 Å) across the face sharing octahedra allow the overlap of wave-functions between these metal centers and thus the direct exchange between moments. Such direct Cr^{3+}–Cr^{3+} interaction is antiferromagnetic resulting from two t_{2g} orbitals after Kanamori and Goodenough's rules [32]. Another important point is that only finite chains or fragments of chains occur along the *c*-axis; (iv) indirect exchange: all $Cr_{5-x}Ti_xTe_8$ phases were reported metallic [13], so the RKKY indirect exchange interaction should be included. Depending on the separation between a pair of ions their magnetic coupling can be FM or antiferromagnetic; (v) double exchange and/or charge ordering: within the frame of an ionic picture, the electronic situation requires the coexistence of Cr^{3+} (d^3) and Cr^{4+} (d^2) for $x \leqslant 1$ and a more complex situation including Ti^{4+} (d^0), Ti^{3+} (d^1), Cr^{3+} (d^3), and Cr^{2+} (d^4) for $x \geqslant 1$. Hence, a double-exchange mechanism may exist and lead to FM exchange interactions; (vi) randomness of Cr and Ti distribution. The role of the randomness is crucial for the generation of spin-glass behavior.

For m-Cr_5Te_8, there is a competition between spin-glass order and long-range FM order. This means that there is a majority of FM couplings between the individual spins but a sufficiently large number of antiferromagnetic couplings (for example, from the interlayer Cr–Cr direct exchange) to create substantial frustration. When the temperature is lowered, a transition from PM to FM and on further lowering the temperature typical spin glass behavior appears which is commonly called RSG behavior.

For m-$Cr_{4.5}Ti_{0.5}Te_8$ and m-Cr_4TiTe_8, the increase of Ti content first leads to the decrease of T_c. The substitution of Cr by Ti and their random distribution then weaken the intra-layer FM superexchange and may break it up, thus forming the CG below T_c. For these two compounds, FM interactions are still dominant.

In m-$Cr_{3.5}Ti_{1.5}Te_8$ the Cr content is further reduced by Ti, the intra-layer FM interactions are further reduced and weakened and at this stage the inter-layer Cr^{3+}–Cr^{3+} direct antiferromagnetic interaction becomes dominant. Such interactions have a short-range character because they are from the finite chains in the structure.

For tr-$Cr_3Ti_2Te_8$, tr-$Cr_2Ti_3Te_8$, and tr-$Cr_{0.25}TiTe_2$, the concentration of Ti is so high that the intra-layer FM interaction and the inter-layer AF interactions become difficult to keep them in long-range. For these compounds, most of the Cr atoms are isolated or in small clusters. Hence the competition of short-range FM and AFM interactions leads to a magnetic spin-glass state at low temperature.

3.3. Band-structure calculations

3.3.1. Preferential site occupation

Spin polarized scalar-relativistic KKR band structure calculations have been performed for the trigonal $Cr_{5-x}Ti_xTe_8$ ($x = 2-5$) samples in FM state. The structure and the lattice parameters used for these calculations are those determined by experiment (see above). The structure of the trigonal compounds with supercell has been reduced to the CdI_2 structure, with metal atoms on sites 1*a* and 1*b*, and Te atoms on site 2*d*. Due to this structure reduction, the formula is reduced to $(Cr_{1-x}Ti_x)_{1.25}Te_2$. As the experiment shows that the 1*a* layer is fully and the 1*b* layer is partially occupied with metal atoms, we first investigated the preference of the metal atoms occupying the 1*a* or 1*b* layer. We performed calculations of the total energy for the $Ti_{1.25}Te_2$ system when y% of the Ti atoms is moved from 1*a* to 1*b* plane, according to the scheme: $Ti_{1.0}Ti_{0.25}Te_2 \rightarrow Ti^a_{1-y}Ti^b_{0.25+y}Te_2$. As can be seen in Fig. 9, an increase in the total energy of the $Ti_{1.25}Te_2$ system results when moving Ti atoms from the 1*a* to the 1*b* planes. This increase of the total energy with the concentration y is monotonous and nearly linear up to $y = 30\%$. This result confirms the preferential occupation determined by experiment. If the overall concentration of the metal atoms was increasing in this system, the 1*a* plane would be occupied first. Only after the 1*a* plane has been fully occupied, the metal atoms start to populate the 1*b* plane.

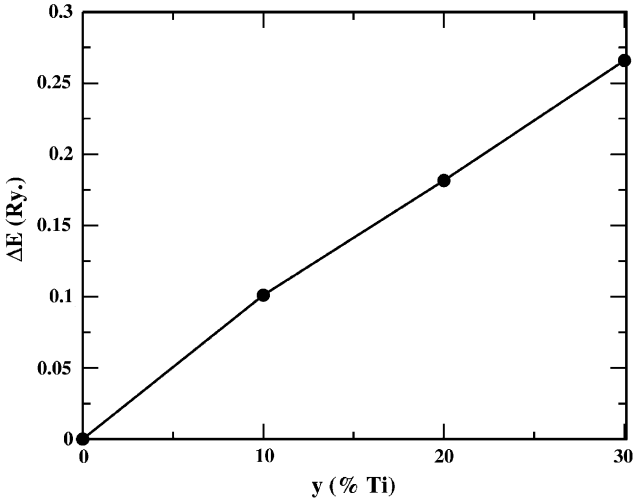

Fig. 9. The SP-SR KKR total energy variation of the system $Ti_{1.25}Te_2$ as a function of Ti concentration y moved from site 1*a* to site 1*b*, according to the scheme: $Ti_{1.0}Ti_{0.25}Te_2 \rightarrow Ti^a_{1-y}Ti^b_{0.25+y}Te_2$.

Secondly, the preference of the Cr and Ti atoms for one of the two layers was questioned. This preference must be energetically determined and it must be reflected in the variation of the total energy if a certain percentage of Cr/Ti is moved from the 1*a* to the 1*b* layer. We have started by supposing that the distribution is statistical and the occupancy of a certain site (1*a* or 1*b*) is proportional to the concentration of Cr/Ti in the compound. This means that for $Cr_{0.25}Ti_{1.0}Te_2$, the occupation is given by the formula $(Cr_{0.20}Ti_{0.80})^a(Cr_{0.05}Ti_{0.20})^bTe_2$. We suppose now that a certain percentage (denoted by δ) of Ti atoms is moved from site 1*a* to site 1*b*, according to the scheme: $(Cr_{0.20}Ti_{0.80})^a(Cr_{0.05}Ti_{0.20})^bTe_2 \rightarrow (Cr_{0.20+\delta}Ti_{0.80-\delta})^a(Cr_{0.05-\delta}Ti_{0.20+\delta})^bTe_2$. The KKR results for the variation of the total energy with δ (the percentage of Ti moved from site 1*a* to site 1*b*) are shown in Fig. 10. The total energy of the system $Cr_{0.25}Ti_{1.0}Te_2$ increases if Ti is moved from site 1*a* to site 1*b*. The system with the lowest energy (for $\delta = -0.20$) is described by the formula: $Ti^a_{1.0}Cr^b_{0.25}Te_2$. This result reflects the preference of Ti atoms for site 1*a* and respectively of Cr atoms for site 1*b*. Calculations performed for the other systems of $(Cr_{1-x}Ti_x)_{1.25}Te_2$ type with $x = 0.4$ and $x = 0.6$ give similar results.

3.3.2. Density of states and magnetic moments

The spin-resolved density of states for the system $Cr_{0.25}Ti_{1.0}Te_2$ is presented in Fig. 11. The main features

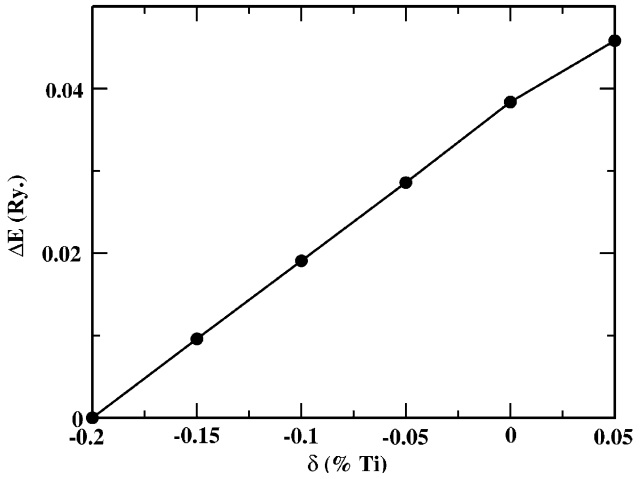

Fig. 10. The SP-SR KKR total energy variation of the system $Cr_{0.25}Ti_{1.0}Te_2$ as a function of Ti concentration δ moved from site 1*a* to site 1*b*, according to the scheme: $(Cr_{0.20}Ti_{0.80})^a(Cr_{0.05}Ti_{0.20})^bTe_2 \rightarrow (Cr_{0.20+\delta}Ti_{0.80-\delta})^a(Cr_{0.05-\delta}Ti_{0.20+\delta})^bTe_2$.

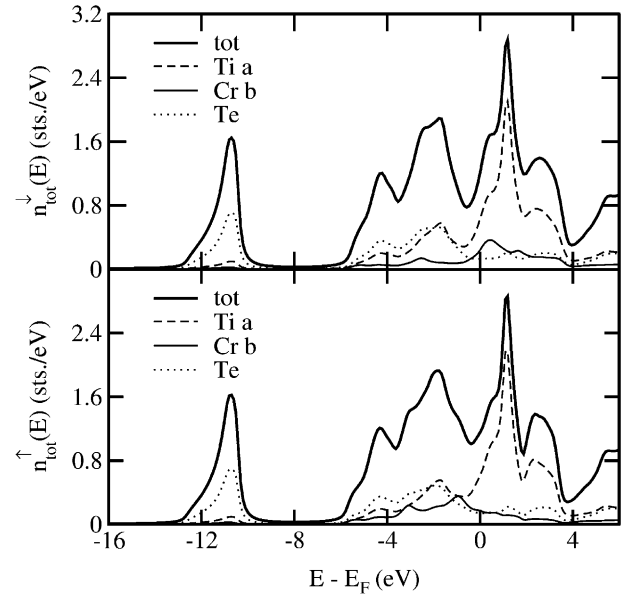

Fig. 11. Spin-resolved DOS of the system $Cr_{0.25}Ti_{1.0}Te_2$ obtained by KKR calculations. The Fermi level is the origin of the energy scale.

of the KKR calculated DOS of these systems are similar to the ASW calculations of Dijkstra et al. [3(h), (j)] for CrTe compounds with a NiAs-like structure. Note that the total DOS in Fig. 11 is represented by a concentration-weighted sum of each component of local DOS. The band at around −12 eV has *s*-anion origin, whilst the higher energy band crossing the Fermi level has Cr/Ti(3*d*)–Te(*p*) character. In the lower part of the *d*–*p* band the influence of the exchange-splitting is minor. A small exchange-splitting in the upper part of the *d*–*p* band is visible due to the Cr(3*d*) states. The magnetic moments for trigonal $(Cr_{1-x}Ti_x)_{1.25}Te_2$ systems obtained by spin polarized scalar-relativistic KKR band-structure calculations are presented in Table 5. As can be seen, the magnetic moment of Cr on site 1*b* is about 25% smaller than the magnetic moment on site 1*a*. Also, an increase of the magnetic moments on 1*b* site occurs with the Cr content of the system. The magnetic moments of Cr on the 1*a* sites are almost independent of the Cr content of the system. On the Ti sites, on the other hand, there is a small induced magnetic moment. We should also note the magnitude and the sign of the magnetic moment on the Te atoms. Their magnetic moments are antiparallel with the Cr/Ti moments and their magnitude increases with the Cr content. This negative magnetic polarization is ascribed by Dijkstra et al. [3(h)] in the case of Cr–Te compounds to the covalent mixing of Cr 3*d* and Te *p*-bands.

Table 5
Spin magnetic moments (μ_B) in trigonal $(Cr_{1-x}Ti_x)_{1.25}Te_2$ compounds

	$Cr_{0.25}Ti_{1.0}Te_2$	$Cr_{0.5}Ti_{0.75}Te_2$	$Cr_{0.75}Ti_{0.5}Te_2$
Cr 1*a*	—	3.09	3.07
Ti 1*a*	0.06	0.06	0.09
Cr 1*b*	2.33	2.39	2.46
Te 2*d*	−0.01	−0.06	−0.10

4. Conclusion

The substitution of the Cr by Ti in Cr_5Te_8 has been realized in the whole concentration range. An intermediate structural modification with a trigonal supercell occurs between monoclinic Cr_5Te_8 and Ti_5Te_8 with a trigonal basic cell. The structures of $Cr_{5-x}Ti_xTe_8$ ($x = 0$, 0.5, 1.0, 1.5, 1.85, 2.0, 3.0, 4.0, 5.0) phases prepared by the slow cooling mode are different from those reported previously, which were synthesized by the quenching mode. The dilution of Cr by Ti in Cr_5Te_8 first leads to a decrease of T_c. Increasing the number of Ti atoms, the 2D intra-layer FM interactions and the inter-layer AF interactions of finite chains are suppressed. The competition of FM and AFM interactions plays the central role in the transition from the re-entrant ferromagnet m-Cr_5Te_8, first to the cluster-glasses m-$Cr_{4.5}Ti_{0.5}Te_8$ and m-Cr_4TiTe_8, then to antiferromagnetic m-$Cr_{3.5}Ti_{1.5}Te_8$, and finally to the spin-glasses tr-$Cr_3Ti_2Te_8$, tr-$Cr_2Ti_3Te_8$, and tr-$Cr_{0.25}TiTe_2$. SP-SR KKR band-structure calculations yield the results consistent with the observation of preferential site occupation of transition metal in the full metal layers from the Rietveld refinements. These calculations predict that Ti atoms have the preference for the sites in the full metal layers, and that these compounds are metallic. Neutron scattering experiments are scheduled to determine the metal atom (Cr/Ti) distribution and the magnetic

structures. The investigation of the possibility of phase transition by DSC and high-temperature X-ray diffraction experiments between monoclinic and trigonal modifications is also planned.

Acknowledgments

The authors thank Dr. R.K. Kremer (MPI Stuttgart) and Dr. H. Pausch (University of Kiel) for their help in magnetic measurements and Mr. H. Hartl (LMU-Munich) for chemical analysis (ICP). The DFG is acknowledged for the financial support of SPP 1136 project (BE 1653/12-1).

References

[1] (a) J. Dijkstra, C.F. Van Bruggen, C. Haas, R.A. de Groot, Phys. Rev. B 40 (1989) 7973–7976;
(b) M.S. Park, S.K. Kwon, S.J. Youn, B.I. Min, Phys. Rev. B 59 (1999) 10018–10024;
(c) W.H. Xie, Y.Q. Xu, B.G. Liu, D.G. Pettifor, Phys. Rev. Lett. 91 (2003) 037204-1–037204-4;
(d) W.H. Xie, B.G. Liu, D.G. Pettifor, Phys. Rev. B 68 (2003) 134407-1–134407-7.

[2] (a) I.F.K. Lotgering, E.W. Gorter, J. Phys. Chem. Solids 3 (1957) 238–249;
(b) D. Babot, M. Chevreton, J. Solid State Chem. 8 (1973) 175–181;
(c) M. Yuzuri, K. Segi, Physica B 86–88 (1977) 891–892;
(d) Y. Ueda, K. Kosuge, M. Urabayashi, A. Hayashi, S. Kawano, J. Solid State Chem. 56 (1985) 263–267;
(e) Y. Sugimoto, S. Ohta, S. Yuri, M. Tamaki, S. Anzai, J. Phys. Soc. Japan 54 (1985) 3240–3243;
(f) S. Ohta, J. Phys. Soc. Japan 54 (1985) 1076–1086;
(g) K. Hatakeyama, S. Ohta, T. Kaneko, H. Yoshida, S. Abe, S. Anzai, J. Phys. Soc. Japan 63 (1985) 4163–4168;
(h) M. Yuzuri, T. Kanomata, T. Kaneko, J. Magn. Magn. Mater. 70 (1987) 223–224;
(i) M. Yuzuri, M. Sato, J. Magn. Magn. Mater. 70 (1987) 221–222;
(j) S. Anzai, H. Sakamoto, K. Hatakeyama, S. Ohta, S. Ichikawa, J. Phys. Soc. Japan 59 (1990) 1059–1070;
(k) Adachi, M. Yuzuri, T. Kaneko, S. Abe, J. Magn. Magn. Mater. 104 (1992) 887–888;
(l) Y. Hinatsu, T. Tsuji, K. Ishida, J. Solid State Chem. 120 (1995) 49–53;
(m) H. Saito, V. Zayets, S. Yamagata, K. Ando, Phys. Rev. Lett. 90 (2003) 207202-1–207202-4.

[3] (a) H. Haraldsen, E. Kowalski, Z. Anorg. Allgem. Chem. 224 (1935) 329–336;
(b) H. Haraldsen, A. Neuber, Z. Anorg. Allgem. Chem. 234 (1937) 353–371;
(c) K. Ozawa, T. Yoshimi, M. Irie, S. Yanagisawa, Phys. Stat. Sol. 11 (1972) 581–588;
(d) J.M. Leger, J.P. Bastide, Phys. Stat. Sol. 29 (1975) 107–113;
(e) M. Yuzuri, T. Kanomata, T.J. Kaneko, J. Magn. Magn. Mater. 70 (1987) 223–224;
(f) K. Hatakeyama, T. Kaneko, H. Yoshida, S. Ohta, S. Anzai, J. Magn. Magn. Mater. 90–91 (1990) 175–176;
(g) T. Kanomata, Y. Sugawara, K. Kamishima, H. Mitamura, T. Goto, S. Ohta, T. Kaneko, J. Magn. Magn. Mater. 177–181 (1998) 589–590;
(h) J. Dijkstra, H.H. Weitgering, C.F. van Bruggen, C. Haas, R.A. de Groot, J. Phys.: Condens. Matter 1 (1989) 9141–9161;
(i) J. Dijkstra, C.F. van Bruggen, C. Haas, R.A. de Groot, J. Phys.: Condens. Matter 1 (1989) 9163–9174.

[4] (a) M. Chevreton, M. Murat, C. Eyraud, J. Phys. 24 (1963) 443–446;
(b) A.W. Sleight, T.A. Bither, Inorg. Chem. 8 (1969) 566–569;
(c) M. Yuzuri, J. Phys. Soc. Japan 35 (1973) 1252;
(d) T. Kaneko, J. Sugawara, K. Kamigaki, S. Abe, H. Yoshida, J. Appl. Phys. 53 (1982) 2223–2225;
(e) Y. Adachi, M. Yuzuri, T. Kaneko, S. Abe, H. Yoshida, J. Phys. Soc. Japan 63 (1994) 369–370;
(f) Adachi, M. Ohashi, T. Kaneko, M. Yuzuri, Y. Yamaguchi, S. Funahashi, Y. Morii, J. Phys. Soc. Japan 63 (1994) 1548–1559.

[5] (a) H. Harldsen, A. Neuber, Naturwissenschaften 24 (1936) 280;
(b) M. Yuzuri, Y. Nakamura, J. Phys. Soc. Japan 19 (1964) 1350–1354;
(c) T.J.A. Popma, C.F. Van Bruggen, J. Inorg. Nucl. Chem. 31 (1969) 73–80;
(d) K. Dwight, N. Menyuk, A. Kafalas, Phys. Rev. B 2 (1970) 3630–3633;
(e) T.J.A. Popma, C. Haas, B. van Laar, J. Phys. Chem. Solids 32 (1971) 581–590;
(f) D. Babot, M. Chevreton, J. Solid State Chem. 8 (1973) 166–174;
(g) M. Yuzuri, T. Kaneko, T. Tsushima, S. Miura, S. Abe, G. Kido, N. Nakagawa, J. Phys. C 8 (1988) 231–232;
(h) J. Hibble, R.I. Walton, D.M. Pickup, J. Chem. Soc. Daltons Trans. (1996) 2245–2251;
(i) P. Vaqueiro, A.V. Powell, A.I. Coldea, C.A. Steer, M.I. Marshall, S.J. Blundell, I. Singleton, T. Ohtani, Phys. Rev. B 64 (2001) 132402-1–1-132402-4.

[6] W. Bensch, O. Helmer, C. Naether, Mater. Res. Bull. 32 (1997) 305–318.

[7] H. Huppertz, H. Luehmann, W. Bensch, Z. Naturforsch. 58b (2003) 934–938.

[8] W. Bensch, H. Luehmann, C. Naether, H. Huppertz, Z. Kristallogr. 217 (2002) 510–514.

[9] K. Lukoschus, S. Kraschinski, C. Naether, W. Bensch, J. Solid State Chem. 177 (2004) 951–959.

[10] Z.-L. Huang, W. Bensch, D. Benea, H. Ebert, J. Solid State Chem. 177 (2004) 3245–3253.

[11] H. Cordes, R. Schmid-Fetzer, J. Alloys Compd. 216 (1994) 197–206.

[12] D.K.G. De Boer, C.F. Van Bruggen, G.W. Bus, R. Coehoorn, C. Haas, G.A. Sawatzky, H.W. Myron, D. Norman, H. Padmore, Phys. Rev. B 29 (1984) 6797–6809.

[13] K. Hatakeyama, A. Takase, S. Anzai, H. Yoshida, T. Kaneko, S. Abe, S. Ohta, Jpn. J. Appl. Phys. 39 (2000) 507–510.

[14] J. Rodriguez-Carvajal, Fullprof. 2k, Version 2.0c, July 2002/Lab. Leon Brillouin, 2002.

[15] A. Gonis, Green Functions for Ordered and Disordered Systems, North-Holland, Amsterdam, 1992.

[16] P. Weinberger, Electron Scattering Theory for Ordered and Disordered Matter, Oxford University Press, Oxford, 1990.

[17] P. Strange, Relativistic Quantum Mechanics, Cambridge University Press, Cambridge, 1988.

[18] H. Ebert, in: H. Dreyssé (Ed.), Electronic Structure and Physical Properties of Solids, Springer, Berlin, 2000, pp. 191–246.

[19] S.H. Vosko, L. Wilk, M. Nusair, Can. J. Phys. 58 (1980) 1200–1211.

[20] P. Soven, Phys. Rev. 156 (1967) 809–813.

[21] J.S. Faulkner, G.M. Stocks, Phys. Rev. B 21 (1980) 3222–3244.

[22] R.D. Shannon, Acta Crystallogr. A 32 (1976) 751–767.

[23] (a) H. Nakazawa, M. Saeki, M. Nakarina, J. Less-Common Met. 40 (1975) 57–63;
(b) S. Brunie, M. Chevreton, C. R. Acad. Sci. Paris 258 (1964) 5847–5850;
(c) S. Brunie, M. Chevreton, Bull. Soc. Fr. Mineral. Crystallogr. 91 (1967) 422–427;
(d) W. Bensch, J. Koy, Inorg. Chim. Acta 206 (1993) 221–223.
[24] (a) W. Bensch, B. Sander, O. Helmer, C. Näther, F. Tuczek, A.I. Shames, A.M. Panich, J. Solid State Chem. 145 (1999) 235–246;
(b) W. Bensch, B. Sander, R.K. Kremer, W. Kockelmann, J. Solid State Chem. 158 (2001) 198–207.
[25] K. Shimada, T. Saitoh, H. Namatame, A. Fujimori, S. Ishida, S. Asano, S. Anzai, Phys. Rev. 53 (1996) 7673–7683.
[26] (a) S. Mitsuda, H. Yoshizawa, Phys. Rev. 45 (1992) 9788–9797;
(b) W. Abdul-Razzaq, J.S. Kouvel, Phys. Rev. 35 (1987) 1764–1767.
[27] J.G. Park, Y. Jo, J. Park, H.C. Kim, H.-C. Ri, Sh. Xu, Y. Moritomo, S.-W. Cheong, Physica B 328 (2003) 90–94.
[28] Y. Iijima, Y. Kamei, N. Kobayashi, J. Awaka, T. Iwasa, S. Ebuisu, S. Chikazawa, S. Nagata, Philos. Mag. 83 (2003) 2521–2530.
[29] M. Gabay, G. Toulouse, Phys. Rev. Lett. 47 (1981) 201–203.
[30] J.A. Mydosh, Spin Glasses: An Experimental Introduction, Taylor & Francis, London, 1993.
[31] (a) X.G. Li, X.J. Fang, G. Ji, W.B. Wu, K.H. Wong, C.L. Choy, H.C. Ku, J. Appl. Phys. 85 (1999) 1663–1666;
(b) S. Mukherjee, R. Ranganathan, P.S. Anikumar, P.A. Joy, Phys. Rev. 54 (1996) 9267–9274;
(c) D.N.H. Nam, K. Jonason, P. Nordblad, N.V. Khiem, N.X. Phuc, Phys. Rev. 59 (1999) 4189–4194;
(d) M. Koyano, M. Suezawa, H. Watanabe, M. Inoue, J. Phys. Soc. Japan 63 (1994) 1114–1122;
(e) A. Maignan, C. Martin, F. Damay, B. Raveau, Phys. Rev. 58 (1998) 2758–2763;
(f) D.A. Pejakovic, J.L. Manson, J.S. Miller, A.J. Epstein, J. Appl. Phys. 87 (2000) 6028–6030;
(g) D.A. Pejakovic, J.L. Manson, J.S. Miller, A.J. Epstein, Phys. Rev. Lett. 85 (2000) 1994–1997;
(h) D.X. Li, A. Donni, Y. Kimura, Y. Shiokawa, Y. Homma, E. Yamamoto, T. Honma, Y. Onuki, J. Phys.: Condens. Matter 11 (1999) 8263–8274.
[32] (a) J. Kanamori, J. Phys. Chem. Solids 10 (1959) 87–98;
(b) J.B. Goodenough, J. Phys. Rev. 100 (1955) 564–573;
(c) J.B. Goodenough, J. Phys. Chem. Solids 6 (1958) 287–297;
(d) J.B. Goodenough, J. Phys. Chem. Solids 30 (1969) 261–280.